Chebyshev neural network-based model for dual-junction solar cells

Patra, Jagdish Chandra

2011

Patra, J. C. (2011). Chebyshev Neural Network-Based Model for Dual-Junction Solar Cells. IEEE Transactions on Energy Conversion, 26(1), 132-139.

https://hdl.handle.net/10356/94347

https://doi.org/10.1109/TEC.2010.2079935

Chebyshev Neural Network-Based Model for Dual-Junction Solar Cells

Jagdish Chandra Patra, *Member, IEEE*

***Abstract*—Design and development process of solar cells can be greatly enhanced by using accurate models that can predict their behavior accurately. Recently, there has been a surge in research efforts in multijunction (MJ) solar cells to improve the conversion efficiency. Modeling of MJ solar cells poses greater challenges because their characteristics depend on the complex photovoltaic phenomena and properties of the materials used. Currently, several commercial complex device modeling software packages, e.g., ATLAS, are available. But these software packages have limitations in predicting the behavior of MJ solar cells because of several assumptions made on the physical properties and complex interactions. Artificial neural networks have the ability to effectively model any nonlinear system with complex mapping between its input and output spaces. In this paper, we proposed a novel Chebyshev neural network (ChNN) to model a dual-junction (DJ) GaInP/GaAs solar cell. Using the ChNN, we have modeled the tunnel junction characteristics and developed models to predict the external quantum efficiency, and *I–V* characteristics both at one sun and at dark levels. We have shown that the ChNN-based models perform better than the commercial software, ATLAS, in predicting the DJ solar cell characteristics.**

***Index Terms*—Chebyshev neural networks (ChNN), dual-junction (DJ) solar cell, modeling, tunnel junction (TJ).**

I. Introduction

AVAILABILITY of effective modeling techniques to accurately estimate the device behavior is quite important to enhance the design and development process of solar cells. In the case of analytical modeling, complex mathematical equations are derived based on materials properties, e.g., optical absorption, hole and electron mobilities, various energy parameters, and physical and chemical phenomena and interactions. Several analytical modeling techniques based on complex mathematical expressions to estimate the behavior of the solar cells have been reported. Some of the recently published reports are modeling of departure of *I–V* characteristics under extreme conditions [1], modeling for intermediate band solar cells [2], modeling of monolithic InGaN/Si two-junction solar cells [3], degradation modeling of InGaP/GaAs/Ge solar cells [4], modeling of solar cells under solar concentration [5], and numerical simulation of tunnel diodes [6]. The aim of electrical solar cell modeling is to develop a link between analytical modeling based on materials properties and the electrical device characteristics. The solar cell is represented by an electrical circuit with series and shunt resistances and a diode. The *I–V* characteristics of the solar cell can be simulated using the electrical circuit parameters. The main solar cell parameters, e.g., the open-circuit voltage (V_{OC}), short-circuit current density (J_{SC}), fill factor (FF), external quantum efficiency (EQE), and conversion efficiency (η), can be obtained from the simulated *I–V* characteristics. Using a network model, Burgelman *et al.* have reported an effective modeling technique for nanostructured solar cells [7]. Simulation and optimization of metal–insulator–semiconductor inversion-layer silicon solar cells using 2-D numerical modeling and circuit simulation have been reported in [8]. In addition, several commercial complex device modeling software packages based on different analytical and electrical modeling techniques are available [9], [10].

These modeling techniques are based on the mathematical relationships and interactions that depend on physical, chemical, and electronic properties of the materials used in the solar cells. Although these techniques provide adequate solutions in most of the devices, they may not yield accurate results in case of complex multijunction (MJ) solar devices. One of the main reasons for the inadequacy of analytical or electrical techniques is due the fact that some of the complex phenomena and material properties are not well known, e.g., the band-to-band recombination, Shockley–Read–Hall scattering time, absorption coefficients for different materials, reflective and resistive losses, etc. [3]. Therefore, several assumptions and simplifications are made in the modeling techniques that lead to inaccuracies in the predicted device behavior.

Artificial neural networks (ANNs), due to their several unique attributes, e.g., ability to learn, adapt and generalize, and tolerance to noise and faults, have been successfully used to solve several complex and highly nonlinear problems [11]. A multilayer perceptron (MLP) trained with back-propagation (BP) algorithm is one of the most popular ANNs that has been used in several applications.

Wide application of ANNs and artificial intelligence techniques for photovoltaic (PV) modeling is evident from the excellent review paper [12]. Recently, Abdulhadi *et al.* [13] have used a neurofuzzy-based model to predict the I_{SC} and V_{OC} of solar cells. A radial basis function (RBF)-based controller to increase PV plant efficiency [14], ANN-based characterization of Si-crystalline PV modules [15], and ANN techniques for accurate estimation of electrical circuit parameters [16] have been reported with impressive results. Some other applications of ANNs include estimation of maximum power generation in PV modules [17], prediction of maximum power point of PV

The author is with the School of Computer Engineering, Nanyang Technological University, Singapore, Singapore (e-mail: aspatra@ntu.edu.sg).

systems using improved RBF networks [18] and PV system design [19].

Difficulties associated with measurement and characterization of tunnel diodes and MJ solar cells have been reported by Guter and Bett [20]. A 3-D-distributed model for high-concentrator solar cells based on elementary units made up of electrical circuits is presented in [21]. Baudrit and Algora [22] modeled a GaInP/GaAs DJ solar cell and tunneling phenomenon using the device simulator ATLAS from Silvaco [9]. They have shown that the ATLAS is able to provide satisfactory performance in predicting tunneling behavior, determination of EQE, and *I–V* characteristics of the dual-junction solar cell under solar irradiation and darkness. However, the ATLAS results are not accurate enough to match to that of measured ones. Substantial deviations are found between the experimental and the ATLAS-simulated results for the FF and conversion efficiency computed from the *I–V* characteristics of the DJ cell.

A functional link ANN (FLANN) is a highly effective and computationally efficient, and the fast learning single layer ANN in which the hidden layer is replaced by a functional expansion block for enhancement of the input pattern space [23]. The Chebyshev neural network (ChNN) is one class of the FLANN in which functional expansion is carried out using orthogonal Chebyshev polynomials that is computationally more efficient than the popularly used MLP networks. The ChNN has been successfully applied in intelligent sensors [24], digital communication [25], and dynamic system identification [26]. In this paper, we proposed ChNN-based models to characterize a DJ GaInP/GaAs solar cell. We have shown that in comparison to the ATLAS model, the ChNN-based model is able to predict the DJ solar cell parameters more closely to that of the experimental ones. In this paper, we have taken the data (experimental and simulated through the ATLAS) from the article reported by Baudrit and Algora [22].

The rest of this paper is organized as follows. The basic theory of the ANN-based modeling scheme from a system identification perspective is given in Section II. The results of the ChNN-based model for estimation of tunnel junction (TJ) characteristics and its performance comparison with the experimental and ATLAS simulated results are provided in Section III. In the next section, we provide results of the ChNN-based model for estimation of EQE and *I–V* characteristics of the DJ solar cell, both under one sun and in darkness, and computed the FF and conversion efficiency. Performance comparison with experimental and the ATLAS-simulated results, and the sensitivity analysis of ChNN-based models are also provided. We provide conclusion and few comments for further study in Section V.

II. System Identification and Chebyshev Neural Network

Identification of an unknown system is an important task in control of industrial plants and prediction and estimation of parameters in any process or system. The pioneer work of Narendra and Parthsarathy [27] has shown the effectiveness of the ANN-based identification of nonlinear dynamic systems. In an earlier paper [26], we have reported the ability of the ChNN for identification of nonlinear dynamic systems. Here, we briefly describe the system identification perspective of a solar cell modeling, explain the theory of the ChNN and the learning algorithm, based on our earlier paper [26].

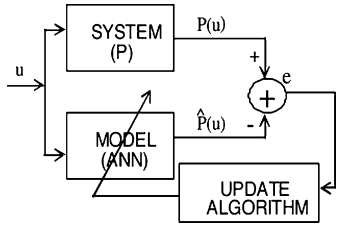

Fig. 1. Schematic of system identification.

A. Characterization and Identification of Systems

Let the model of a system is represented by an operator $\mathbf{P}$ that transforms the input space $\mathcal{U}$ into an output space $\mathcal{Y}$. The operator $\mathbf{P}$ is defined implicitly by the specified input–output pairs. The objective is to categorize the class $\mathcal{P}$ to which $\mathbf{P}$ belongs. For a given class $\mathcal{P}$, $\mathbf{P} \in \mathcal{P}$, the identification problem is to determine a class $\hat{\mathcal{P}} \subset \mathcal{P}$ and $\hat{\mathbf{P}} \in \hat{\mathcal{P}}$ such that $\hat{\mathbf{P}}$ approximates $\mathbf{P}$ in some desired sense. In a static system, the spaces $\mathcal{U}$ and $\mathcal{Y}$ are subsets of $\mathcal{R}^n$ and $\mathcal{R}^m$, respectively [**?**]. Pattern recognition is an example of the static identification problem. Using a decision function $\mathbf{P}$, input sets $U_i \subset \mathcal{R}^n$ are mapped into elements $y_i \in \mathcal{R}^m$ for $i = 1, 2, \ldots$, in the output space. The elements of U_i denote the pattern vectors corresponding to class y_i. The main objective is to determine $\hat{\mathbf{P}}$ such that

$$\|y - \hat{y}\| = \|\mathbf{P}(u) - \hat{\mathbf{P}}(u)\| < \epsilon \tag{1}$$

where $u \in \mathcal{U}$, ϵ is some desired small value > 0, and $\|\cdot\|$ is a defined norm on the output space. In (1), $\hat{\mathbf{P}}$ and $\mathbf{P}$ denote the output of the identified model and the plant, respectively. The error, $e = y - \hat{y}$, is the difference between the observed plant output and the output generated by the model.

In the schematic diagram of the system identification shown in Fig. 1, the input and output of the plant are represented by u and $\mathbf{p}(u)$, respectively, where u is assumed to be a uniformly bounded function of time. The objective is to construct a suitable model generating an output $\hat{\mathbf{P}}(u)$ that approximates the plant output $\mathbf{P}(u)$. In the context of solar cell modeling, we consider the plant to be the solar cell in which the input–output relationship is represented by a nonlinear function given by

$$y_p(k) = f(u(k)) \tag{2}$$

where $u(k)$ and $y_p(k)$ represent the input and the output of a solar cell at the kth time instant, respectively. In this paper, we used a ChNN to construct the nonlinear function $f(.)$ by using several measurement data as training set. For modeling TJ characteristics, the model input and output are given by the input voltage and the tunnel diode current, respectively, whereas, for estimation of EQE of the DJ solar cell, the model's input and output are given by the radiation wavelength and EQE, respectively.

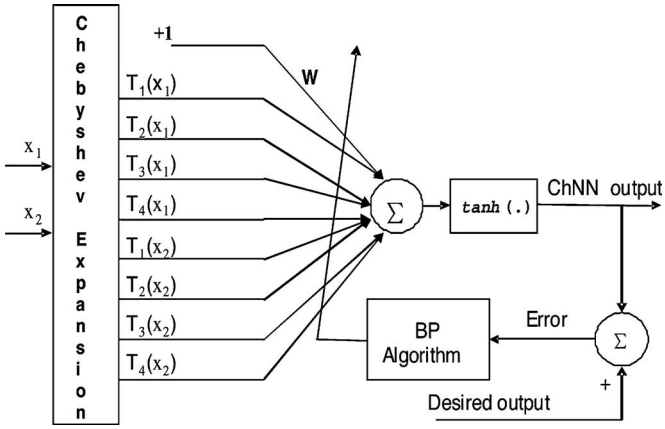

Fig. 2. Schematic of a Chebyshev neural network.

B. ChNN

The structure of a ChNN is depicted in Fig. 2. It consists of a functional expansion block and a single-layer perceptron network. The main purpose of the functional expansion block is to increase the dimension of the input pattern so as to enhance its representation in a higher dimensional space. This enhanced pattern is then used for modeling of the solar cell. Let us denote an n-dimensional input pattern at kth instant by

$$X_k = [x_1(k), x_2(k), \ldots, x_n(k)]^T. \tag{3}$$

Each element of the input vector is expanded to several terms using Chebyshev polynomials. The Chebyshev polynomials are a set of orthogonal polynomials obtained as a solution of the Chebyshev differential equation. The rth-order Chebyshev polynomial is denoted by $T_r(x)$, where $-1 < x < 1$. The first few Chebyshev polynomials are given by

$$\begin{aligned} T_0(x) &= 1 \\ T_1(x) &= x \\ T_2(x) &= 2x^2 - 1 \\ T_3(x) &= 4x^3 - 3x \\ T_4(x) &= 8x^4 - 8x^2 + 1. \end{aligned} \tag{4}$$

The higher order Chebyshev polynomials may be generated using the recursive formula

$$T_{r+1}(x) = 2xT_r(x) - T_{r-1}(x). \tag{5}$$

Using the Chebyshev polynomials, an n-dimensional input pattern is expanded to an l-dimensional ($l > n$) enhanced pattern, which is then applied to a single-layer perceptron. In the ChNN schematic shown in Fig. 2, the values of n and l are 2 and 9, respectively. The advantage of the ChNN over MLP is that the Chebyshev polynomials are computationally more efficient and takes much less time to train compared to an MLP network.

C. Learning of ChNN

The learning process involves updating of the weights (W) of the ChNN in order to minimize a given cost function. A gradient descent algorithm is used for learning where the gradient of a cost function with respect to the weight is determined and the weights are incremented by a fraction of the negative gradient at each iteration. The well-known BP algorithm [11] is used to update the weights of the ChNN. Considering the single-output ChNN as shown in Fig. 2, its output is given by

$$y = \tanh(s) \tag{6}$$

where the linear sum s is given by

$$s = \sum_{i=1}^{l} w_i T_i(X) \tag{7}$$

where $X \in \mathcal{R}^n$, $X = [x_1, x_2, \ldots, x_n]^T$ is the input vector, $T_i(X), \{i = 1, 2, \ldots, l\}$, is an element of the expanded input vector and $W = [w_1, w_2, \ldots, w_l]^T$ is the weight vector of the ChNN.

The learning algorithm minimizes E_k, the cost function at kth instant

$$E_k = \frac{1}{2}[d_k - y_k]^2 = \frac{1}{2}e_k^2 \tag{8}$$

where d_k is the desired output at the kth instant, and e_k denotes the error term. In each iteration, an input pattern is applied, the output of the ChNN is computed, and the error e_k is obtained. The error value is then used in the BP algorithm to minimize the cost function until it is less than a predefined small value. The weights are updated as follows:

$$W_{k+1} = W_k + \triangle W_k = W_k + \left(-\alpha \frac{\partial E_k}{\partial W_k}\right) \tag{9}$$

where the learning parameter α is set between 0 and 1. The gradient of the cost function (8) is given by

$$\frac{\partial E_k}{\partial W} = e_k \frac{\partial y_k}{\partial W}. \tag{10}$$

The update rule for the weight w_i is given by

$$w_{i,k+1} = w_{i,k} + e_k \frac{\partial y_k}{\partial w_i}. \tag{11}$$

Since $\tanh(.)$ function is used at the output node, the update rule becomes

$$w_{i,k+1} = w_{i,k} + \alpha e_k (1 - y_k)^2 T_i(X). \tag{12}$$

To improve convergence, a momentum term is added to the update rule as follows:

$$w_{i,k+1} = w_{i,k} + \alpha \triangle w_{i,k} + \beta \triangle w_{i,k-1} \tag{13}$$

where the momentum factor β is set between 0 and 1.

The mean square error (MSE) during training in dB at the kth iteration is defined as

$$\text{MSE}_{\text{train}}(k) = 10\log 10 \left(\frac{1}{N_p N_L} \sum_{p=1}^{N_p} \sum_{i=1}^{N_L} \left[e_i^{(p)}(k) \right]^2 \right) \tag{14}$$

where N_p denotes the number of training patterns used. In this paper, the number of output nodes $N_L = 1$.

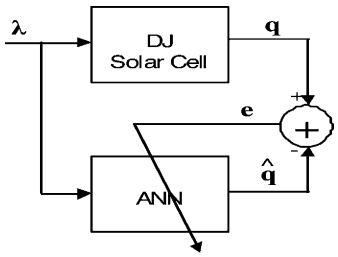

Fig. 3. ANN-based schematic diagram for estimation of external quantum efficiency of a DJ solar cell.

D. Estimation of Solar Cell Characteristics

An ANN-based schematic diagram to estimate the EQE of a DJ solar cell is shown in Fig. 3. The input to the ANN is the wavelength (λ) of irradiation and its target output is the measured EQE (q). A set of input and target output (taken from the experimental measurements) is given to the ANN during the training phase. After application of each input, the ANN computes its output ($\hat{q}$) that is then compared with the target output to produce an error. This error is used in the BP algorithm to update the weights of the ANN. After a sufficient number of iterations, the MSE (14) between the target and ANN outputs settles down to a minimum value. Thus, the training of the ANN is completed and now the ANN is ready for estimation of solar cell's EQE. In a similar way, for estimation of the TJ and *I–V* characteristics, different sets of input-target data sets are used during training of the ANN.

III. Modeling of Tunnel Junction Characteristics

One of the reasons of the lack of accurate modeling techniques for MJ solar cells is due to the difficulties in modeling of highly complex phenomena in tunnel diodes. Here we provide modeling of a tunnel diode using a the ChNN. For this modeling purpose, we have taken the experimental and ATLAS-simulated data form [22].

A. Principles of Tunneling Phenomenon

In a highly doped p–n junction, tunneling of charge carriers through the bandgap is an important part of transport mechanism. The two fundamental tunneling mechanisms in a p–n junction are: 1) the direct transition from band to band and 2) the transition via traps, i.e., trap-assisted tunneling (TAP). A schematic of the two tunneling mechanisms is shown in Fig. 4. The principles of band-to-band tunneling phenomenon can be explained by using the Kane model [28] in which the tunneling current through a potential barrier is described analytically. The tunneling probability for charge carriers in a parabolic potential barrier is given by

$$T_t \approx \exp\left(-2\int_{r_1}^{r_2}\left[\frac{2m}{h^2}(V(r)-E)\right]^{1/2} dr\right) \qquad (15)$$

where r_1 and r_2 are the turning points of the wave functions, m is the tunneling mass, and $V(r)$ is the potential barrier. The tunneling current can be computed using the Fermi–Dirac distribution $f_C(E)$ and $f_V(E)$, and the density states of the electrons $D_n(E)$ and holes $D_p(E)$, as follows:

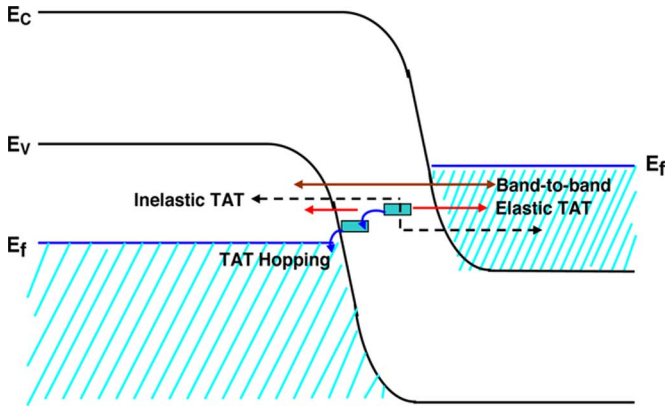

Fig. 4. Schematic of tunneling mechanisms.

$$J_t \propto \int_{E_C}^{E_V} [f_C(E) - f_V(E)]\, T_t D_n(E) D_p(E) dE. \qquad (16)$$

From (16), one can see that the tunneling current depends on the tunneling probability and the supplied functions for the electrons and holes. These are implemented in device simulators for numerical simulation of the tunneling current. The device simulator computes the carrier transport in the device by solving the electron–hole continuity equations and the Poisson equation. The tunneling mechanism is incorporated by an additional recombination term in the continuity equation that is done by adopting either a local or a nonlocal tunneling model [6].

B. Performance Comparison

In order to compare the performance of the ATLAS-modeled tunneling behavior, an isolated p^{++}-GaAS/n^{++}–GaAS tunnel diode grown by the metal organic vapour phase epitaxy (MOVPE) technique has been investigated. The simulated TJ structure used in the ATLAS is shown in Fig. 5 [22]. The tunnel diode consists of a TJ made by two degenerately doped p^{++}- and n^{++}-GaAS layers along with two enclosing barrier layers, in order to minimize the doping effect. The CAP and the substrate layers were also included in the simulation. Local and nonlocal TAT tunneling mechanisms have been included in the simulation using the ATLAS. The results of the ATLAS-simulated TJ characteristics and the experimentally measured values are plotted in Fig. 6. It can be seen that the ATLAS response and experimental values match quite closely.

In our ChNN-based model, the 1-D input pattern was expanded to a 12-D pattern (including bias unit) by using Chebyschev polynomials. Thus, the ChNN architecture is represented as $\{12–1\}$. We selected 60% of the experimentally measured data points as training set to train the ChNN. The input voltage (V) and the tunnel diode current (A/cm^2), respectively, were used as input and target output to the ChNN. Both the input and target output to the ChNN were normalized between -0.9 and 0.9. The learning parameter α and momentum factor β used in the BP algorithm were selected as 0.16 and 0.5,

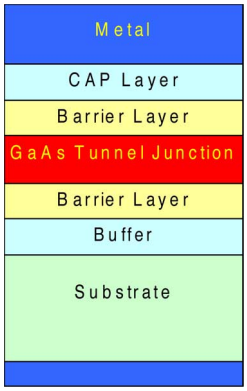

Fig. 5. TJ structure used in ATLAS simulation.

respectively, after several experiments to give the best results. The training continued for 50 000 iterations that resulted in an MSE (14) value of -27.8 dB. To verify the effectiveness of the ChNN-based model, the whole measured data set was applied to the trained ChNN. The TJ characteristics estimated by the ChNN-based model are shown in Fig. 6.

To determine effectiveness of the models quantitatively, we computed correlation coefficient (CC) between the experimental and the model-predicted outputs. The CC between the experimental and ChNN outputs is denoted as CC_{ChNN}, and the CC between the experimental and ATLAS outputs is denoted as CC_{ATLAS}. Another quantitative measure we used for performance comparison is the MSE between the experimentally measured data and the estimated output from the ATLAS simulator or the ChNN-based model. The MSE in dB between the experimental data and the ATLAS data is given by

$$\text{MSE}_{\text{ATLAS}} = 10\log10\left(\frac{1}{N}\sum_{i=1}^{N}[x_i - y_i]^2\right) \qquad (17)$$

where x_i and y_i denote the experimental and ATLAS-estimated data, respectively. Similarly, MSE_{ChNN} is defined.

The estimated characteristics and scatter plot along with the CC and MSE performances of the ChNN-based model are also shown in Fig. 6. It can be seen that the ChNN-based model provides better performance than the ATLAS model in terms of both CC and MSE.

IV. Modeling of the DJ Solar Cell

In this paper, the main objective of simulation of the tunnel diode is to use the TJ as an interconnection between the subcells of a DJ solar cell. After successful modeling of TJ characteristics, we study further to develop the ChNN-based models for the DJ solar cell. For this purpose, we have investigated a GaInP/GaAs DJ cell simulated by the ATLAS using the layer thickness and doping levels as given in Table I. We used a ChNN-based model to estimate the EQE and *I–V* characteristics both at one sun and dark levels.

After several simulations (as discussed in Section IV-E), we found the optimum parameters of the ChNN as follows: the number of input $N_{\text{input}} = 12$, learning rate, $\alpha = 0.16$, momentum factor, $\beta = 0.5$, the number of iterations, $N_{\text{nitr}} = 50\,000$ and percent of the measurement data used for training $N_{\text{trgsample}} = 60\%$. These optimum values were used in the following sections.

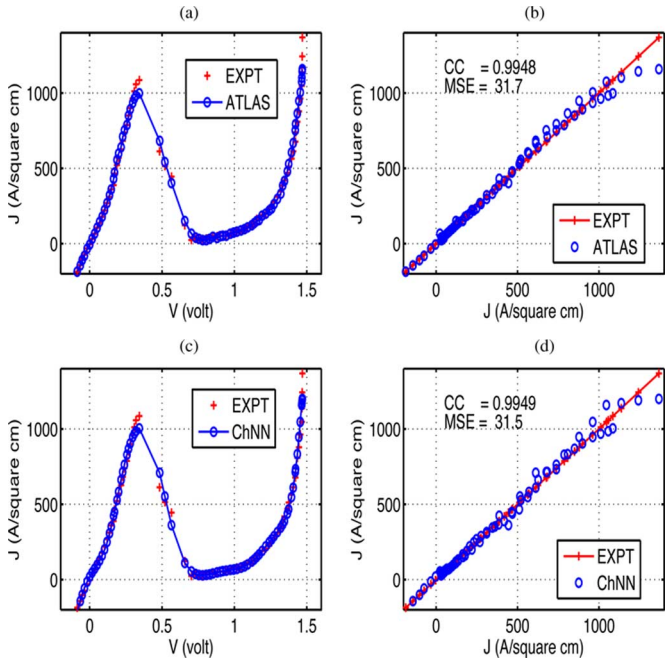

Fig. 6. Estimated TJ characteristics obtained from (a) and (b) ATLAS and (c) and (d) ChNN models.

TABLE I
Structure of the DJ Solar Cell

Sl. No.	Name	Material	Nominal thickness (nm)	Doping concentration (cm^{-3})
1	topfsf	$AlInP$	50	$n = 3.0 \times 10^{+17}$
2	topem	$Ga_{0.51}In_{0.49}P$	170	$n = 1.8 \times 10^{+18}$
3	topbase	$Ga_{0.51}In_{0.49}P$	800	$p = 1.0 \times 10^{+17}$
4	topbsf	$AlGaInP$	100	$p = 3.0 \times 10^{+17}$
5	phighTD	$GaAs$	50	$p = 5.0 \times 10^{+19}$
6	nhighTD	$GaAs$	50	$n = 3.0 \times 10^{+19}$
7	botfsf	$Al_{0.4}Ga_{0.6}As$	50	$n = 2.0 \times 10^{+18}$
8	botem	$GaAs$	100	$n = 1.0 \times 10^{+10}$
9	botbase	$GaAs$	3,500	$p = 2.0 \times 10^{+17}$
10	botbsf	$Al_{0.3}Ga_{0.7}As$	100	$p = 2.0 \times 10^{+18}$
11	subs	$GaAs$	300,000	$p = 2.0 \times 10^{+18}$

A. Modeling of External Quantum Efficiency

The EQE is an important parameter in design and development of solar cells. It depends on the physical properties, structure, and thickness of the materials used, and the incident irradiation wavelength, in a complex manner. The EQE is defined as

$$\text{EQE} = \text{SR}(\lambda)\frac{h\nu}{q} \qquad (18)$$

where $\text{SR}(\lambda)$ is the spectral response (in A/W) at the incident wavelength λ, $h\nu$ is the energy of the incident photon, and q is the electronic charge.

In a GaInP/GaAs DJ cell, due to the resonant cavity effect occurring between the top cell back surface field (BSF) and the bottom cell window layer, the EQE suffers from oscillations in the bottom GaAs cell. In order to accurately model the EQE in a DJ cell, the ATLAS incorporates a characteristics matrix

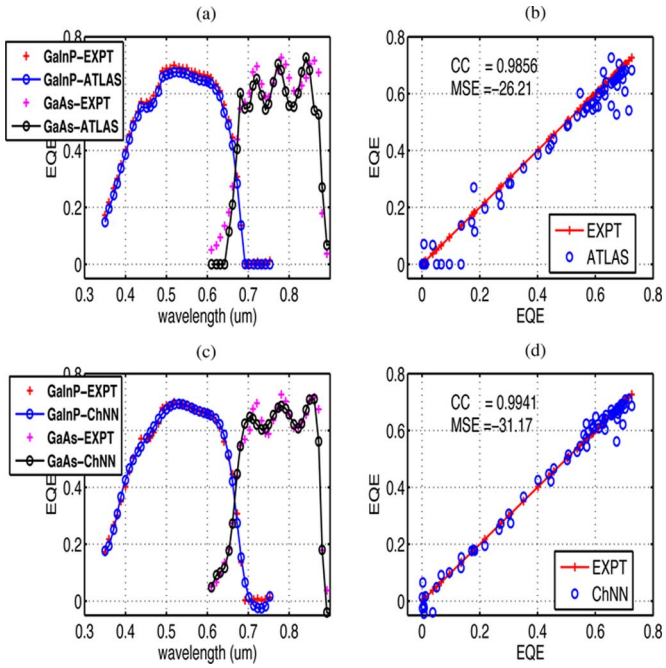

Fig. 7. Estimated EQEs obtained through (a) and (b) ATLAS and (c) and (d) ChNN models.

approach that relates total tangential components of the electric and magnetic fields at the multilayer boundaries [22]. The experimental results and the ATLAS model output are plotted in Fig. 7.

We modeled EQE of the DJ solar cell with a ChNN using the optimum parameters. The radiation wavelength (λ) and the computed EQE from the experimental measurement are the input and the target output to the ChNN, respectively. The training continued for 50 000 iteration to achieve an MSE level (14) of -29.7 dB. After completion of training, all the data points were used to estimate the EQE. The results of the ChNN-based model are also shown in Fig. 7. It can be seen that the ChNN-based model performs better than the ATLAS model in terms of both MSE and CC.

B. Modeling of I–V Characteristics at One Sun

The experimentally measured *I–V* characteristics of the DJ solar cell at one sun along with the ATLAS-simulated characteristics are shown in Fig. 8. It can be seen that there is a good amount of deviation between the two characteristics. We used a two-layer ChNN $\{12\text{–}1\}$ with the optimum parameters to model the *I–V* characteristics. The input and the target output to the ChNN, respectively, were the voltage (in V) and current density (in $\mathrm{mA/cm^2}$). The training data set was applied and updating of ChNN weights were carried out for 50 000 iterations to produce an MSE level (14) of -28.1 dB. The testing of the ChNN was done with all the experimental data. The results of the ChNN model are shown in Fig. 8. The response characteristics of the ChNN model almost overlap the experimental characteristics. This fact indicates the excellent performance of the ChNN model.

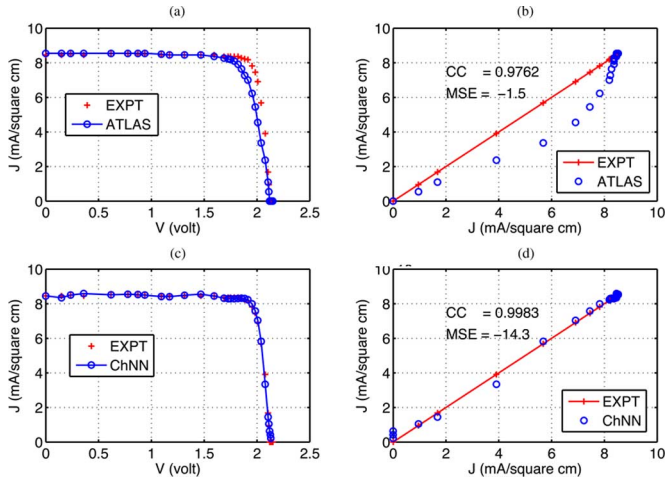

Fig. 8. Estimated *I–V* characteristics at one sun obtained through (a) and (b) ATLAS and (c) and (d) ChNN models.

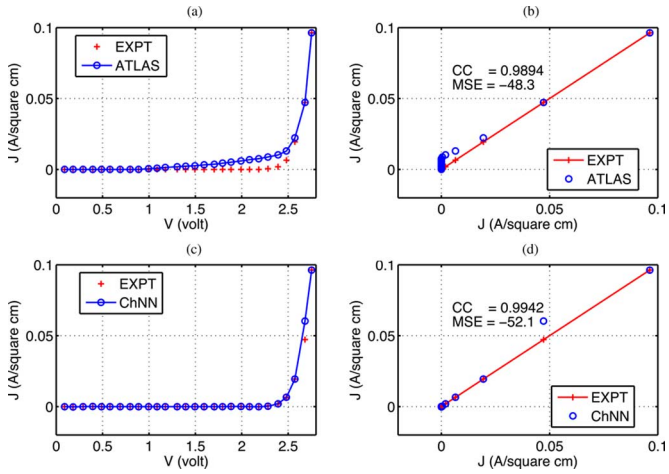

Fig. 9. Estimated *I–V* characteristics at dark obtained through (a) and (b) ATLAS and (c) and (d) ChNN models.

C. Modeling of I–V Characteristics at Dark

The experimentally measured *I–V* characteristics of the DJ solar cell at dark along with the ATLAS-simulated characteristics are shown in Fig. 9. The ChNN was trained in a similar way as that at one sun. Once again, the response of the ChNN model is found to be superior to that of the ATLAS model, in terms of both CC and MSE.

Performance comparison of the ChNN-based models for the DJ solar characteristics is shown in Table II. It can be seen that for all the four DJ solar characteristics the ChNN-based models perform better than the ATLAS model in terms of both CC and MSE.

D. Computation of DJ Solar Cell Parameters

We computed the major parameters the DJ solar cell, e.g., J_{SC}, V_{OC}, FF, and η, from the *I–V* characteristics and these values are tabulated in Table III. It may be noted that the experimentally

TABLE II
PERFORMANCE COMPARISON BETWEEN THE CHNN- AND ATLAS-BASED MODELS

DJ Model	CC $_{ChNN}$	CC $_{ATLAS}$	MSE $_{ChNN}$	MSE $_{ATLAS}$
TJ	0.9949	0.9948	31.50	31.73
EQE	0.9941	0.9856	-31.17	-26.21
IVSun	0.9983	0.9762	-14.30	-1.50
IVDark	0.9942	0.9894	-52.1	-48.27

TABLE III
COMPARISON OF COMPUTED DJ SOLAR CELL PARAMETERS

DJ Parameter	Experimental	ChNN	ATLAS
J_{SC} (mA/cm^2)	8.4	8.4	8.4
V_{OC} (V)	2.12	2.12	2.12
J_{max} (mA/cm^2)	7.9	7.9	7.66
V_{max} (V)	1.9	1.9	1.82
FF (%)	84.28	84.28	78.28
η (%)	15.01	15.01	13.94

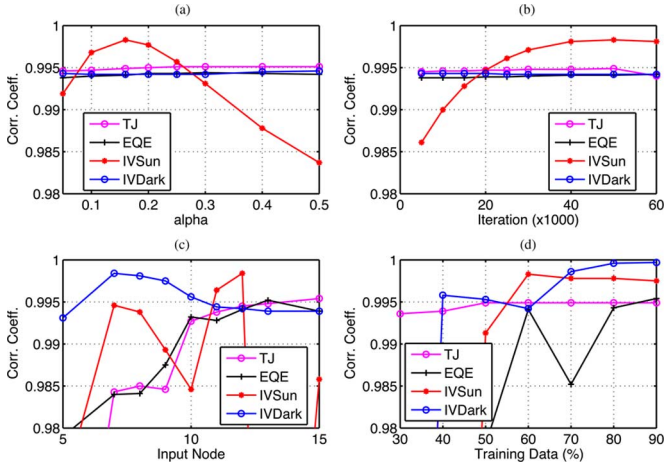

Fig. 10. Sensitivity analysis of ChNN-based models in terms of correlation coefficient. (a) Alpha. (b) Iteration. (c) Input node. (d) Sample data.

measured values were taken under the standard test conditions: the air mass (AM) 1.5 spectrum with an incident power density of 1000 $\mathrm{W/cm^2}$ and a temperature of 25 °C. It can be seen that the parameters obtained through the ChNN-based model match closely to that obtained through experiment.

E. Sensitivity Analysis of ChNN-Based Model

In this section, we study the effect of variation of ChNN parameters on the performance of the ChNN-based model in predicting the DJ solar cell characteristics. We varied the learning parameter (α), number of training iterations N_{nitr}, number of input nodes (N_{input}), and percent of measurement data used for training ($N_{\mathrm{trgsample}}$), one at a time, while keeping the other parameters at their optimum values. The results of this analysis with CC performance measure are shown in Fig. 10.

The four DJ solar cell model characteristics are denoted as TJ (tunnel junction characteristics), EQE, IVSun (*I–V* characteristics at one sun), and IVDark (*I–V* characteristics at dark). For the four characteristics, as α increases from 0.05 to 0.50

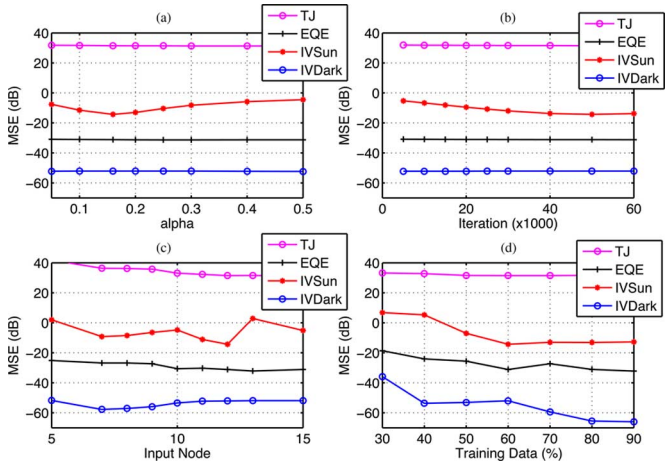

Fig. 11. Sensitivity analysis of ChNN-based models in terms of MSE. (a) Alpha. (b) Iteration. (c) Input node. (d) Sample data.

the CC remains steady about 0.995 for TJ, EQE, and IVDark. However, the IVSun characteristics seem to be quite sensitive to variation of α. The maximum value of CC (0.9983) for IVSun characteristics was obtained at $\alpha = 0.16$. As the number of iterations increased from 5000 to 60 000, the CC increases from 0.9861 to 0.9981 for IVSun characteristics; however, for other three characteristics, it remains steady at 0.995. The influence of the number of input nodes, i.e., the number of functional expansion, is quite prominent for all the four characteristics. It can be seen that the at $N_{\mathrm{input}} = 12$, the CC is optimum for all the four characteristics. Finally, it can be seen that the percent of sample data used for training the ChNN affects the CC performance substantially. The optimum value of CC was obtained when ($N_{\mathrm{trgsample}} = 60\%$). The MSE performance with variation of the ChNN parameters is shown in Fig. 11. At the selected optimum ChNN parameters ($\alpha = 0.16$, $N_{\mathrm{nitr}} = 50\,000$, $N_{\mathrm{input}} = 12$, and $N_{\mathrm{trgsample}} = 60\%$), the MSE performance is found to be quite satisfactory for all the four ChNN models.

V. CONCLUSION

In this paper, we proposed a novel ChNN-based technique for modeling of complex DJ solar cell characteristics. Using single-layer ChNNs, we have modeled the TJ behavior and estimated the EQE and *I–V* characteristics at one sun and dark levels with quite satisfactory results. With extensive computer simulations, we have shown that the ChNN-based models could achieve superior performance than the models generated by the device simulator, the ATLAS by Silvaco [9]. Especially, for the estimation *I–V* characteristics, the ChNN-based models match perfectly to that of the experimental characteristics. The electrical parameters, e.g., J_{SC}, V_{OC}, J_{max}, V_{max}, FF and η, computed from the *I–V* characteristics match closely to those obtained from the experimentally measured characteristics. Due to their low-computational complexity, the ChNNs are preferable in modeling of complex and nonlinear phenomena. Furthermore, because of their flexibility and adaptability, the ANNs can be used for other modeling aspects of MJ solar cells.

ACKNOWLEDGMENT

The author would like to thank the anonymous reviewers whose positive and constructive comments and suggestions helped to enhance the quality of this paper to a great extent.

REFERENCES

[1] A. Cuevas and J. Tan, "Analytical and computer modelling of suns–Voc silicon solar cell characteristics," *Solar Energy Mater. Solar Cells*, vol. 93, pp. 958–960, 2009.

[2] A. S. Lin, W. Wang, and J. D. Phillips, "Model for intermediate band solar cells incorporating carrier transport and recombination," *J. Appl. Phys.*, vol. 105, pp. 064512-1–064512-8, 2009.

[3] L. Hsu and W. Walukiewicz, "Modeling of InGaN/Si tandem solar cells," *J. Appl. Phys.*, vol. 104, pp. 024507-1–024507-7, 2008.

[4] S.-I. Sato, H. Miyamoto, M. Imaizumi, K. Shimazaki, C. Morioka, K. Kawano, and T. Ohshima, "Degradation modeling of InGaP/GaAs/Ge triple-junction solar cells irradiated with various-energy protons," *Solar Energy Mater. Solar Cells*, vol. 93, pp. 768–773, 2009.

[5] A. Cheknane, H. S. Hilal, J. P. Charles, B. Benyoucef, and G. Campet, "Modelling and simulation of InGaP solar cells under solar concentration: Series resistance measurement and prediction," *Solid State Sci.*, vol. 8, pp. 556–559, 2006.

[6] M. Hermle, G. Letay, S. P. Philipps, and A. W. Bett, "Numerical simulation of tunnel diodes for multijunction solar cells," *Progr. Photovoltaics: Res. Appl.*, vol. 16, pp. 409–418, 2008.

[7] M. Burgelman, M. Minnaert, and C. Grasso, "Device modeling of nanostructured solar cells," in *Nanostructural Materials for Solar Energy Conversion*. T. Soga, Ed. Amsterdam, The Netherlands: Elsevier, 2006, pp. 45–80.

[8] B. Kuhlmann, A. G. Aberle, R. Hezel, and G. Heiser, "Simulation and optimization of metal–Insulator–Semiconductor inversion-layer silicon solar cells," *IEEE Trans. Electron. Devices*, vol. 47, no. 11, pp. 2167–2178, Nov. 2000.

[9] SILVACO. [Online]. Available: http://www.silvaco.com/

[10] Synopsys. [Online]. Available: http://www.synopsys.com/tools/tcad/pages/ffdefault.aspx

[11] S. Haykin, *Neural Networks*, 2nd ed. Upper Saddle River, NJ: Prentice-Hall, 1999.

[12] A. Mellita and S. A. Kalogirou, "Artificial intelligence techniques for photovoltaic applications: A review," *Prog. Energy Combustion Sci.*, vol. 34, pp. 574–632, 2008.

[13] M. Abdulhadi, A. M. Al-Ibrahim, and G. S. Virk, "Neurofuzzy-based solar cell model," *IEEE Trans. Energy Convers.*, vol. 19, no. 3, pp. 619–624, Sep. 2004.

[14] A. Varnham, A. M. Al-Ibrahim, G. S. Virk, and D. Azzi, "Soft-computing model-based controllers for increased photovoltaic plant efficiencies," *IEEE Trans. Energy Convers.*, vol. 22, no. 4, pp. 873–880, Dec. 2007.

[15] F. Almonacid, C. Rus, L. Hontoria, M. Fuentes, and G. Nofuentes, "Characterisation of Sicrystalline PV modules by artificial neural networks," *Renew. Energy*, vol. 34, pp. 941–949, 2009.

[16] E. Karatepe, M. Boztepe, and M. Colak, "Neural network based solar cell model," *Energy Convers. Manage.*, vol. 47, pp. 1159–1178, 2006.

[17] T. Hiyama and K. Kitabayashi, "Neural network based estimation of maximum power generation from PV module using environmental information," *IEEE Trans. Energy Convers.*, vol. 12, no. 3, pp. 241–247, Sep. 1997.

[18] C.-C. Liao, "Genetic k-means algorithm based RBF network for photovoltaic MPP prediction," *Energy*, vol. 35, no. 2, pp. 529–536, 2010.

[19] D. Paul, S. N. Mandal, D. Mukherjee, and S. R. B. Chaudhuri, "Artificial neural network modeling for efficient photovoltaic system design," in *Proc. IEEE Intl. Conf. Adv. Comput. Theory Eng.*, Phuket, Thailand, Dec. 2008, pp. 50–56.

[20] W. Guter and A. W. Bett, "*I–V* characterization of tunnel diodes and multijunction solar cells," *IEEE Trans. Electron Devices*, vol. 53, no. 9, pp. 2216–2222, Sep. 2006.

[21] B. Galiana, C. Algora, I. Rey-Stolle, and I. Vara, "A 3-D model for concentrator solar cells based on distributed circuit units," *IEEE Trans. Electron Devices*, vol. 52, no. 12, pp. 2552–2558, Dec. 2005.

[22] M. Baudrit and C. Algora, "Modeling of GaInP/GaAs dual-junction solar cells including tunnel junction," presented at the Proc. 33rd IEEE Photovoltaic Spec. Conf., St. Diego, CA, May 2008.

[23] Y.-H. Pao, *Adaptive Pattern Recognition and Neural Networks*. Reading, MA: Addison-Wesley, 1989.

[24] J. C. Patra, M. Juhola, and P. K. Meher, "Intelligent sensors using computationally efficient Chebyshev neural networks," *IET Sci. Meas. Technol.*, vol. 2, no. 2, pp. 68–75, Mar. 2008.

[25] J. C. Patra, W. B. Poh, N. S. Chaudhari, and A. Das, "Nonlinear chaneel equalization with QAM signal using Chebyshev artificial neural network," in *Proc. IEEE Int. Joint Conf. Neural Netw. (IJCNN'2005)*. Montreal, Canada, Aug. 1995, pp. 3214–3219.

[26] J. C. Patra and A. C. Kot, "Nonlinear dynamic system identification using Chebyshev functional link artificial neural network," *IEEE Trans. Syst., Man, Cybern., Part B-Cybern.*, vol. 32, no. 4, pp. 505–511, Aug. 2002.

[27] K. S. Narendra and K. Parthasarathy, "Identification and control of dynamical systems using neural networks," *IEEE Trans. Neural Netw.*, vol. 1, no. 1, pp. 4–27, Mar. 1990.

[28] E. O. Kane, "Theory of tunneling," *J. Appl. Phys.*, vol. 32, pp. 83–91, 1961.

Jagdish Chandra Patra (M'97) received the Ph.D. degree from Indian Institute of Technology, Kharagpur, India, in 1996.

He was a Reserch Fellow at the School of Electrical and Electronic Engineering, Nanyang Technological University (NTU), Singapore, in 1999. He is currently an Assistant Professor at the School of Computer Engineering, NTU. His research interests include intelligent information processing using neural networks in the areas of information security, sensor networks, image processing, digital communication, bioinformatics and multijunction solar cell modeling. He has more than 100 publications in these areas of research.

Dr. Patra is a member the Institution of Engineers, India.